Article

Not peer-reviewed version

Modification of Pore Wall Surface in Shs-Prepared Porous TiNi for Ophthalmic Orbital Implants

Sergey G. Anikeev *, Valentina N. Hodorenko, Maria I. Kaftaranova, Anastasiia V. Shabalina, Nadezhda V. Artyukhova, Elena N. Terletskaya, Sergei A. Kulinich *, Sofiya Pakholkina, Elena A. Bolshevich, Vladimir Promakhov, Victor E. Gunther, Yuri A. Medvedev

Posted Date: 8 January 2024

doi: 10.20944/preprints202401.0580.v1

Keywords: porous TiNi alloy; ophthalmic orbital implants; powder metallurgy; self-propagating high-temperature synthesis, surface modification; biocompatibility; biointegration

Article

Modification of Pore Wall Surface in SHS-Prepared Porous TiNi for Ophthalmic Orbital Implants

Sergey G. Anikeev [1,2,*], Valentina N. Hodorenko[1], Maria I. Kaftaranova[1], Anastasiia V. Shabalina[1], Nadezhda V. Artyukhova[1], Elena N. Terletskaya[3], Sergei A. Kulinich [4,*], Sofiya Pakholkina [1], Elena A. Bolshevich [1], Vladimir Promakhov [5], Victor E. Gunther [1], and Yuri A. Medvedev [6]

[1] Laboratory of Medical Materials Science, Tomsk State University, 634050 Tomsk, Russia
[2] Institute of Physics, Kazan Federal University, 420008 Kazan, Russia
[3] Kuzbass Regional Clinical Hospital, 650000 Kemerovo, Russia
[4] Research Institute of Science and Technology, Tokai University, Hiratsuka, Kanagawa 259-1292, Japan
[5] Scientific and Educational Center "Additive Technologies", Tomsk State University, 634050 Tomsk, Russia
[6] Department of Oral and Maxillofacial Surgery, Moscow State Medical and Dental University, 127006 Moscow, Russia
* Correspondence: anikeev_sergey@mail.ru (S.G.A.); skulinich@tokai-u.jp (S.A.K.)

Abstract: The study focuses on a novel porous TiNi-based material for ophthalmic orbital implants which was produced by self-propagating high-temperature synthesis (SHS) and, after proper surface modification, possesses a specific microstructure of its surface pores, which makes it attractive for biomedical use in implants. After preparation via SHS, the obtained porous TiNi material was etched in acidic environment, to get rid of its surface Ti_2Ni secondary-phase particles. This was found to improve the material's surface morphology, adding micro-roughness to its macro-rough pores. As a result, cell growth tests conducted on the material demonstrated improved cell adhesion and growth kinetics on such a porous material with improved roughness. Finally, the material was tested *in vivo* as an ophthalmic orbital implant, demonstrating good biocompatibility, good degree of biointegration with surrounding eyeball tissues, and no signs of rejection after as long as 180 days. Thus, the novel porous TiNi-based material shows promise for its use in ophthalmic implantology, for instanse for manufacturing musculoskeletal stumps of the eyeball after evisceration, as it is biocompatible, has a high tissue-implant integration potential and demonstrates reduced risks of exposure and rejection of the implant.

Keywords: porous TiNi alloy; ophthalmic orbital implants; powder metallurgy; self-propagating high-temperature synthesis; surface modification; biocompatibility; biointegration

1. Introduction

Eye evisceration (partial removal of the eyeball) is one of the methods used to eradicate the eyeball defects and the infection for patients with serious oculoorbital injuries, intraocular cancers, and other life-threatening diseases [1–3].The formation of a full-fledged musculoskeletal stump of the eyeball after its removal is a necessary condition for achieving a satisfactory functional and aesthetic effect of subsequent ocular prosthetics and, consequently, effective medical and social rehabilitation of the patient [4–11].

Currently, biological (fat, cartilage, bone, etc.), natural (hydroxyapatite), and synthetic (polymeric, ceramic, metallic, carbon, etc.) orbital implants are used to form the musculoskeletal stump of the eyeball. Certainly, all of them have a number of disadvantages. Biological implants are subject to gradual resorption, and they do not ensure the constancy of the volume and shape of the eyeball stump [12–14], or normal growth of orbital bones in children [15]. Also, the need for bacterial and virological testing of donor material requires compliance with the rules of its conservation and storage, the creation of a network of tissue banks, which significantly increases the cost of treatment. The disadvantages of natural and some synthetic orbital implants (polymeric, ceramic, carbon based, etc.) are their exposure, rejection and deformation [13, 16–25]. Metallic implants were found to be

 doi:10.20944/preprints202401.0580.v1

well-applicable and very promising for use in ophthalmology in general, and for the formation of the full-fledged musculoskeletal stump of the eyeball after its removal, in particular [25].

The use of TiNi implants in ophthalmology was previously described elsewhere [26]. The authors studied in detail TiNi implants for the formation of the musculoskeletal stump of the eyeball in the form of monolithic thread, porous-permeable alloy, fabric, mesh, and fiber. In general, porous surface is considered preferable, even in monolithic implantable structures [1]. Porous alloys based on TiNi are quite widely used as materials for implants. The combination of both high biomechanical and biochemical compatibility of TiNi-based porous materials with body tissues makes it possible to solve highly complex problems in various fields of medicine [1, 27–34]. Biocompatible porous TiNi materials for medical use are typically produced by the self-propagating high-temperature synthesis (SHS) and sintering [33–36]. These methods permit to obtain porous materials with martensitic transformations in a wide temperature range, also with a developed structure of the pore volume, an optimal porosity of 50–70%, and an average pore size of 90–150 μm [25].

Unlike sintering, the SHS method is characterized by the highest energy efficiency. TiNi powders are used during sintering. On the contrary, Ti and Ni powders are used during SHS. The implementation of an exothermic chemical reaction in an argon environment leads to the production of a porous material with a high degree of phase-chemical heterogeneity. Large-sized biocompatible porous materials with a highly porous, permeable three-dimensional macrostructure can be created due to the formation of numerous interconnected pores during layer-by-layer synthesis of the alloy.

It is well-known that the surface of the pore walls of porous TiNi-based alloys obtained by the SHS has a high concentration of Ti_2Ni and $Ti_4Ni_2(O,N,C)$ second-phase particles. Their formation is associated with the high activity of Ti at high temperatures and its segregation on the surface of pore walls [37–40]. Unfortunately, such particles can reduce the mechanical properties of the material, since they are brittle and serve as sites for crack propagation during destruction. Also, these particles are the centers where corrosion begins, thereby their presence reduces corrosion resistance of the material. In the present work, however, we take advantage of their availability to further improve the material surface.

The process of interaction of body tissues with an implanted device is known to be determined by the morphochemical parameters of the surface of the pore walls [41, 42]. When operating inside the body, the pore space of porous implant is filled with living tissues and tissue fluids. It has been experimentally established that the pore size, pore size distribution and morphology of the surface of pore walls have a great effect on the cell culture integration in the pore space of implant material [43–45]. Thus, materials possessing pore walls with microporous structures are more preferable for attachment of cellular cultures. It has increased specific surface area and individual micropores can serve as a nutrient depot [46].

There are certain approaches that can be used to enhance the biocompatibility of the surfaces. For instance, such methods as ion beam and plasma treatment, laser-based surface processing, ion and electronic alloying with Si, Mo, Ta were previously employed to improve the surface of monolithic alloys by applying various protective coatings [47 – 52]. Another approach is based on preparing biodegradable hydroxyapatite films or on adding this compound to powders when a porous material is prepared [53]. However, the use of the above-mentioned modification methods is impossible in the case of porous-permeable materials as some technical limitations can emerge. More specifically, there are difficulties with delivering the modifier substance into the pore volume. Moreover, to accelerate the processes of integration of TiNi-based material with cells, it is necessary not to create protective coatings, but to improve the structure of the pore walls surface and of the macropores volume [25].

In the case of SHS-produced materials, structural improvements are possible due to the presence of open, interconnected pores and the possibility to access into the pore space [27]. Such porous structures could be created using different approaches. For instance, in some works [54–55] a powder of NaCl was used for construction of interconnected pore system with a certain size of pore channels. Highly porous materials (up to 90%) with macropores can be obtained depending on the granulometric composition of NaCl powder. Another approach used for the creation of special

 doi:10.20944/preprints202401.0580.v1

porous space with certain design is application of ultrasonication during SHS process [56]. This was found to reduce the number of cavities and increase the maximum pre-heating temperature without their formation. Additive technologies for manufacturing of porous materials with complex structure of pore channels were also described elsewhere [57, 58]. Such works typically aimed at modifying the macrostructure of the pore space, while the microstructure remained unchanged, thus leading to pronounced phase-chemical heterogeneity.

Here, we propose to form microporous surface on pore walls of porous-permeable TiNi produced via SHS by etching away the above-mentioned second-phase particles inside the pores. This way, the formation of such particles during SHS can be turned from material's weakness to its advantage, if the newly formed structure shows enhanced biocompatibility and bio-integration. So, the creating a larger specific surface area via modification of the material would help increase its adhesive properties for tissue cells. In light of this, the most acceptable etching technique would be applying an aqueous solution of nitric and hydrofluoric acids, which potentially can lead to the formation of a microporous surface on pore walls with micro-sized pores corresponding to the size of etched Ti_2Ni and $Ti_4Ni_2(O,C)$ particles.

Thus, the main goal of this study was to develop a method for modifying the pore space of SHS-generated TiNi material by creating a rough surface on its pore walls. After such a modification, the material should become more suitable for the attachment and development of cell cultures inside its pores. We also aimed to study integration processes in the implant-tissue system using the modified TiNi. The use of this material for implanting will ensure formation of a reliable connection between the implant and the surrounding biological tissues of the eye. To achieve the above-mentioned goals, the present work focused on studying the process of formation of microporous surface of pore walls by etching of Ti_2Ni and $Ti_4Ni_2(O,C)$ particles with sizes of 0.1–5 μm. Therefore, the novelty of this work lies on the simple and effective surface modification approach that permits to enhance the biocompatibility and bio-integration of SHS-produced porous TiNi material. Thus-modified porous TiNi was demonstrated to show promise for its use as ophthalmology implants in the future.

2. Materials and Methods

2.1. Material Preparation

In this work, porous alloys based on TiNi were obtained by the SHS method using titanium and nickel powders. The initial Ti (PTOM, purity of 99.94%), Ni (PNK, purity of 99.90%) powders were dried in a GP-20 dry-heat oven (SKTB SPU, Smolensk, Russia) at a temperature of 85-95 °C for 7 h. Then they were mixed in an equiatomic ratio in a mixer C2K/6 (Techno center, Rybinsk, Russia) for 8 h. The resulting mixture was poured into a quartz flask, compacted for 30 min to a green porosity of 75-80%, and placed in a metal reactor. SHS was carried out in an electric tubular furnace SUOL (Tula-Term, Tula, Russia) in an Ar gas atmosphere (Khimmedsnab, Tomsk, Russia). When the temperature reached 450°C, SHS was initiated by short-circuiting an electrical circuit with a voltage of 220 V at the open end of the Ti-Ni blank. For further studies and use, samples of 4 mm × 4 mm × 35 mm in size were cut from the obtained blanks using an ARTA 123 PRO electrical discharge machine (NPK "Delta-Test", Fryazino, Russia).

2.2. Modification of the Material

The resulting porous material was treated by chemical etching with solutions of nitric and hydrofluoric acids diluted with distilled water in a ratio of 1:1:3. Both acids, nitric (65%) and hydrofluoric (45%), were chemically pure and were purchased from Sigmatek (Khimki, Russia). The etching time was 7–10 s at a temperature of 20°C. The etching process occurred in several stages. The experimental sample was immersed in the solution for 2–3 s, taken out for 5 s and immersed again until the time spent in the solution reached 7–10 s. This was done because the treatment was accompanied by abundant gas evolution and there might be a difference in the degree of etching in the center and at the periphery of the sample.

 doi:10.20944/preprints202401.0580.v1

The immersion time was selected experimentally. The etching stages were studied by observing the structural features of experimental samples after etching. The first stage took about 2–3 s, and then the second and third and fourth ones took 3–7, 7–10, and more than 10 s, respectively. After etching, the samples were thoroughly rinsed and immersed in water for 12 h.

2.3. Sample Characterization

Metallographic studies were carried out using an Axiovert-40MAT optical microscope (Carl Zeiss, Oberkochen, Germany). The features of the microstructure and chemical composition of the alloys were studied on a scanning electron microscope SEM 515 (Philips, Amsterdam, the Netherlands) with an EDAX ECON IV microanalyzer (EDAX, Mahwah, NJ, USA). The phase composition was studied using X-ray diffraction analysis on a Shimadzu XRD 6000 diffractometer (Shimadzu, Kyoto, Japan). The size of pores and interpore bridges was determined by a combination of the secant method and the inscribed sphere method. Based on the obtained data, size distribution histograms of pores and interpore bridges were constructed. Porosity was determined by weighing using a GH-200 balance (A&D, Tokyo, Japan). Permeability was determined using the Darcy formula [25]:

$$K = \frac{Q\mu L}{\rho g \Delta H S_0 \Pi},$$

where Q is the fluid flow rate proportional to the density of the fluid (ρ) and inversely proportional to its viscosity (μ); L is the length of the sample; ΔH is the fluid level; g is the gravitational acceleration; S_0 is the cross-sectional area of the sample; and Π is porosity. The permeability coefficient was calculated in three perpendicular directions.

2.4. Cell Development Processes

All procedures involving animals were carefully carried out following strictly the Declaration of Helsinki of 1975, and in accordance with the European Community's Council Directive 86/609/EEC. The study protocol was officially approved (approval code number 20/1116/2017 of May 5, 2017) by the Bioethical Committee of Tomsk State University. Bone marrow stem cells of F1 CBA/j hybrid mice were used as cellular material. The femur was removed under sterile conditions, after which the bone marrow was washed out with a syringe into vials.

Before seeding the cells, they were sterilized at 180°C for 60 min. Cultivation was performed in the following medium: DMEM-F12 medium (PanEco, Moscow, Russia), 10% fetal calf serum (HyClone, USA), gentamicin 40 μg/ml (PanEco, Moscow, Russia), and glutamine 250 mg/l (PanEco, Moscow, Russia). Differentiation additives (beta-glycerophosphate 3 mg/ml (Sigma-Aldrich, St. Louis, USA) in a combination with 0.15 mg/ml ascorbic acid (Sigma-Aldrich, St. Louis, USA) were used in the system with osteogenic differentiation.

The cell concentration was adjusted to 10^7 cells/ml of final medium. The cells were inoculated on TiNi incubators and placed in 50 ml plastic bottles from Corning, Arizona, USA. Incubators with cells were kept at a temperature of T = 37 °C and 100% humidity with a 5% concentration of CO_2.

Samples of porous incubators were removed from the experiment and examined on days 1, 7, 14, and 21. After the removal, they were fixed for 1 h in 2.5% glutaraldehyde (Sigma-Aldrich, St. Louis, USA), then washed 3 times in PBS (15 min each), then fixed for 1 h in 1% osmium tetroxide (Sigma-Aldrich, St. Louis, USA), washed 3 times in PBS, and then dehydrated by passing through a series of ethanol solutions (30, 50, 70, 90, and 100%) for 15 min each. Each incubator sample was examined using a Quanta 200 3D scanning electron microscope (FEI, Hillsboro, USA).

2.5. Evisceration of the Eyeball

All procedures involving animals were carefully carried out with strict adherence to the Helsinki Declaration of 1975 and in accordance with the European Community's Council Directive 86/609/EEC. The study protocol was officially approved (approval code number 138/1 of 16 March 2023) by the Bioethical Committee of Kuzbass Regional Clinical Hospital. The process of biointegration of an orbital implant made of modified porous TiNi was studied in *in-vivo* experiment

 doi:10.20944/preprints202401.0580.v1

on 20 animals (dogs). Anesthesia of laboratory animals participating in the experiment was carried out by intravenous administration of a solution of sodium thiopental (Sintez, Kurgan, Russia) combined with local infiltration anesthesia with a 2% solution of lidocaine hydrochloride (Grotex, Moscow, Russia).

Evisceration of the eyeball was performed according to the standard technique [5]. An orbital implant was immersed into the prepared and properly treated scleral cavity, and scleral flaps were sutured in pairs with U-shaped sutures. Continuous sutures were placed in layers on Tenon's capsule, subconjunctiva and conjunctiva. The operation was completed with an antibiotic injection. Antibacterial therapy was carried out for 7 days. Animals were removed from the experiment by intravenous administration of a 10% lidocaine solution on days 10, 30, 90, and 180. Samples were removed from the animals and immersed in formaldehyde for further studies.

Orbital implant samples were dried on filter paper at room temperature, then placed on stages with electrically conductive tape for fixation, and loaded into the microscope column. The study of experimental samples was carried out on a Quanta 200 3D microscope (FEI, Hillsboro, USA) in a low-vacuum mode (at a pressure P = 70 Pa) using an LFD (Large Field Detector) for working with biological objects. The spatial resolution in this research mode, according to the microscope's passport data, was 15 nm. The focal length was 10–20 mm, the tilt angle of the object stage was 0°. The accelerating voltage was 10–20 kV with the magnification from 36 to 15,000 times. Quantitative analysis of the chemical composition of tissues was performed using a microanalyzer EDAX ECON IV (EDAX, Mahwah, USA) with a silicon detector with a resolution of 120 eV. The state of the fibroformation process on the surface and on the chip of orbital implants was assessed by the microstructure of biological tissue.

3. Results

3.1. Structural Studies of TiNi Material before and after Modification

3.1.1. Macro- and Micro-Porous Structure and Permeability of Material

To be used as implant in ophthalmology, a porous material needs high enough permeability. The latter is necessary for fibrovascular tissue penetration through its interrelated network of pores (which anchors the orbital implant), as well as for the formation of vascular resource required for low postoperative contagion and stimulation of soft tissue healing [1].

The pore space of the SHS-produced TiNi material is seen in Figure 1 to be characterized by a complex structure of interconnected pores. Due to the layer-by-layer synthesis regime applied, the resultant porous-permeable material contains a high fraction of open pores. For such materials, their permeability coefficient is determined by the longitudinal or transverse direction of a liquid passing through the sample. For the TiNi porous alloy obtained in this work, its permeability coefficient values were found to be 588D (standard deviation σ=8D) and 793D (σ=16D) for its two longitudinal directions, and 254D (σ=9D) for its transverse direction. Thus, after its preparation, the material exhibits good permeability, being highly permeable in its both longitudinal directions and medium permeable in its transverse direction. And since the material was prepared by SHS, some anisotropy in its pore space structure is seen based on its permeability coefficients.

Preprints (www.preprints.org) | NOT PEER-REVIEWED | Posted: 8 January 2024 doi:10.20944/preprints202401.0580.v1

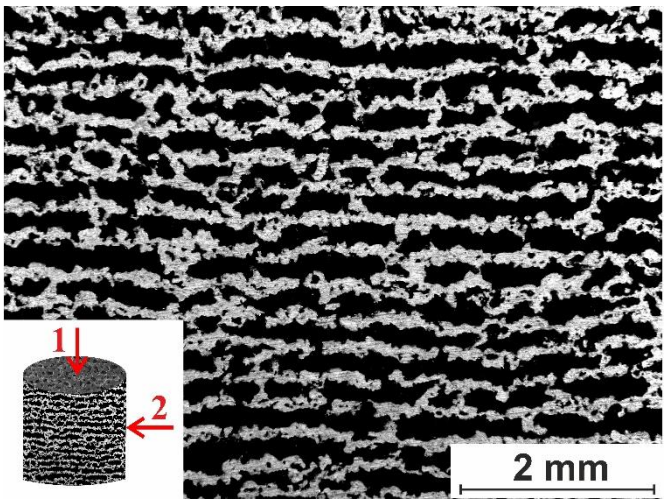

Figure 1. SEM image (BSE mode) of a thin section of porous SHS-prepared TiNi alloy showing macrostructure of the pore space. In inset: 1 is for longitudinal direction, and 2 for transverse direction.

Along with permeability, there are several other parameters that strongly affect material's applicability as implant in ophthalmology. Among such properties that directly influence the process of bio-integration of cellular structures with the implant are the porosity index, pore size distribution, average size and topography of the pore wall surface. Figure 2a shows that the as-prepared TiNi material had a well-developed three-dimensional surface with a network of open and interconnected pores. Its porosity before modification was 64%, and its histogram of pore size distribution was unimodal, which is typical for finely porous materials (Figure 2b). The average pore size was found to be around 175 μm, with the majority of pores being below 200 μm, and the maximum pore size not exceeding 1000 μm.

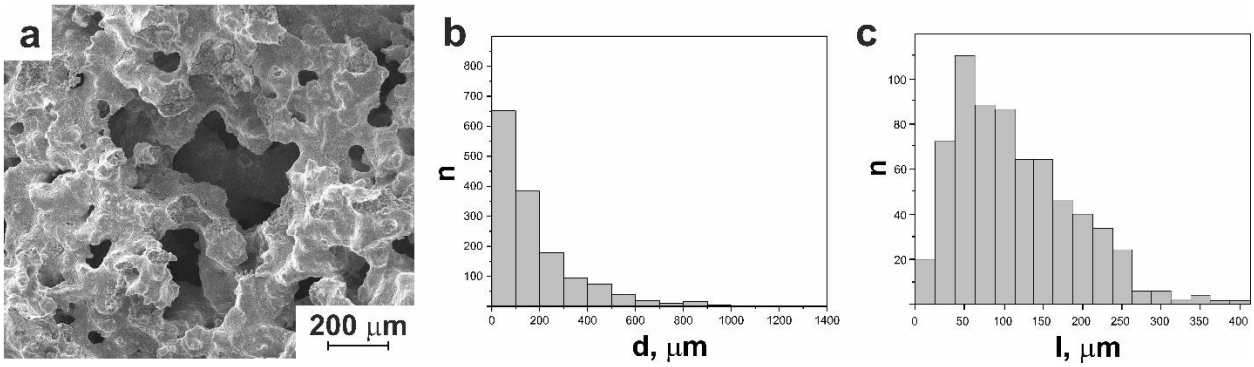

Figure 2. (**a**) SEM image (SE mode) showing surface morphology of porous SHS-prepared TiNi alloy. (**b**,**c**) Histograms of pore size (**b**) and of interpore bridge size (**c**) distribution in the porous TiNi alloy.

During SHS process, the formation of porous space is known to depend much on adsorbed gases which are filtered through the reacting zone of the sample [33, 38, 59, 60]. Intense gas release within the combustion wave occurring during exothermic reactions between Ti and Ni contributes to a temperature elevation in the zone where the structure is formed. This increases the amount of eutectic melt that intensively wets the powder mixture and promotes pore coalescence. With an excess amount of the melt, interpore bridges can increase to 300–350 μm. In the as-prepared TiNi reported here, the average size of such interpore bridges was found to be 127 μm (Figure 2c).

The images of fractured interpore bridges in Figures 3a and 3b show the presence of a surface layer containing light elements C and O. While the porous material was prepared in an inert argon environment, its precursor Ti and Ni powders contacted with the air, which explains the presence of carbon and oxygen in the final product. During high-temperature synthesis, Ti exhibits high activity

Preprints (www.preprints.org) | NOT PEER-REVIEWED | Posted: 8 January 2024 doi:10.20944/preprints202401.0580.v1

and segregates onto free surfaces where it can be partially oxidized in presence of various gases and form compounds with carbon and oxygen. In parallel, after the passage of the combustion wave, when the product crystallizes, a lot of slag is displaced onto the surface of the pore space. After the product is formed, such aggregations are located unevenly on its pore wall surfaces, along with second-phase particles that are known to form in TiNi materials during crystallization.

As found by means of a mercury porosimeter, the as-produced material contained a small number of micropores in its structure (Figure 3c), with the maximum size of such pores being over 10 μm, while smaller pores were barely observed. So, the initial SHS-produced TiNi was a macroporous (with the majority of its pores sizing around 200 μm), mainly highly permeable material with just a small amount of micropores larger than 10 μm. Besides, its pore wall surface contained numerous inclusions of secondary phases obtained during synthesis.

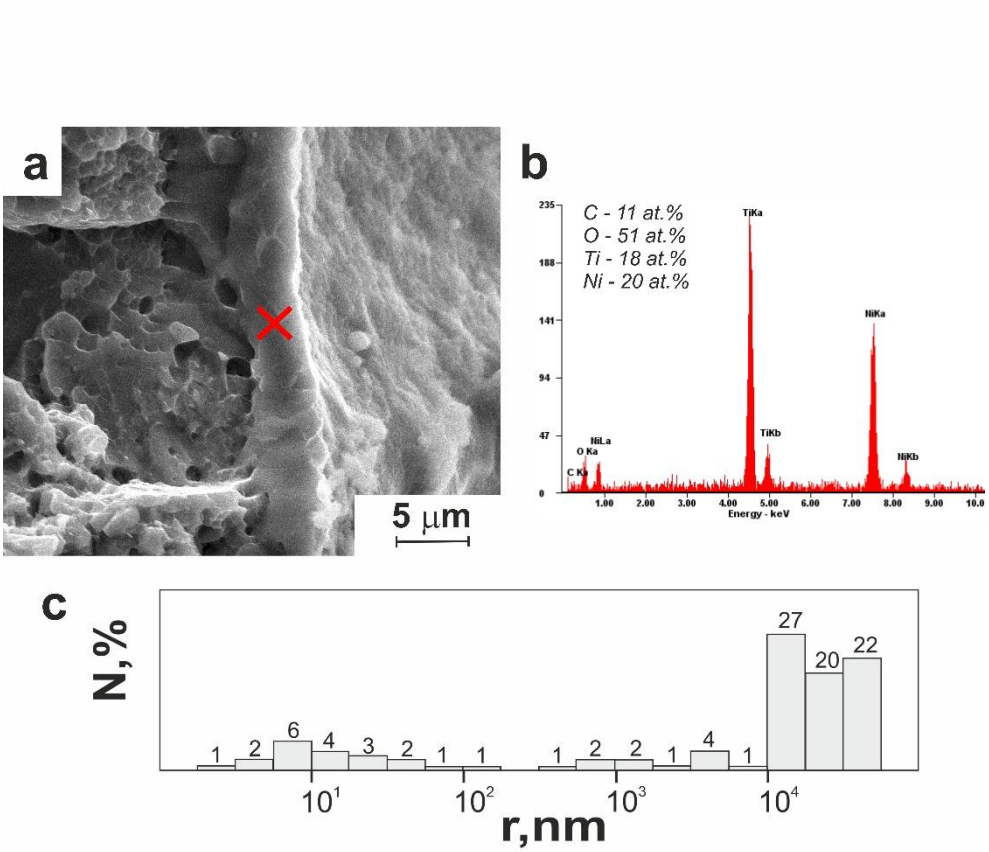

Figure 3. (**a**) SEM image (SE mode) showing a fractogram of destructed interpore bridge of porous SHS-prepared TiNi alloy; (**b**) EDX spectrum of the surface layer of the interpore bridge (taken at the point marked with cross in panel (**a**)); (**c**) histogram of micropore size distribution for the same sample.

3.1.2. Surface Phase Composition

Normally, porous TiNi-based alloys obtained by the SHS method are known for their pronounced heterogeneity. They typically demonstrate abundance of secondary phases, which is due to the short-time processes of reaction diffusion taking place in the zone of structure formation. X-ray diffraction analysis of our as-prepared material confirmed the presence of TiNi (B2, 56 vol.%), TiNi (B19′, 21 vol.%), Ti_2Ni (18 vol.%), and $TiNi_3$ (5 vol.%) phases (Figure 4a).

Typically, the formation of Ti-rich phases occurs at temperatures around 1115 °C during crystallization in accordance with the peritectic reaction [29]. As mentioned above, the powders of Ti

Preprints (www.preprints.org) | NOT PEER-REVIEWED | Posted: 8 January 2024 doi:10.20944/preprints202401.0580.v1

and Ni actively adsorb significant amounts of oxygen and carbon. During the SHS process, such light elements are known to actively enter into diffusion processes and form oxycarbide phases of the $Ti_4Ni_2(O,C)$ type [27]. This type of phases can hardly be distinguished from the Ti_2Ni phase since their crystallographic lattices are very similar ($a(Ti_2Ni)$ = 11.278 Å, while $a(Ti_4Ni_2(O,N,C))$ = 11.328 Å). However, they can be recognized by their shape. The particles containing interstitial elements (C, O) are larger in size and rectangular, diamond-shaped or triangular, whereas Ti_2Ni particles are smaller in size and have irregular rounded contours. Nevertheless, for brevity, hereafter all these phases will be denoted as Ti_2Ni-type.

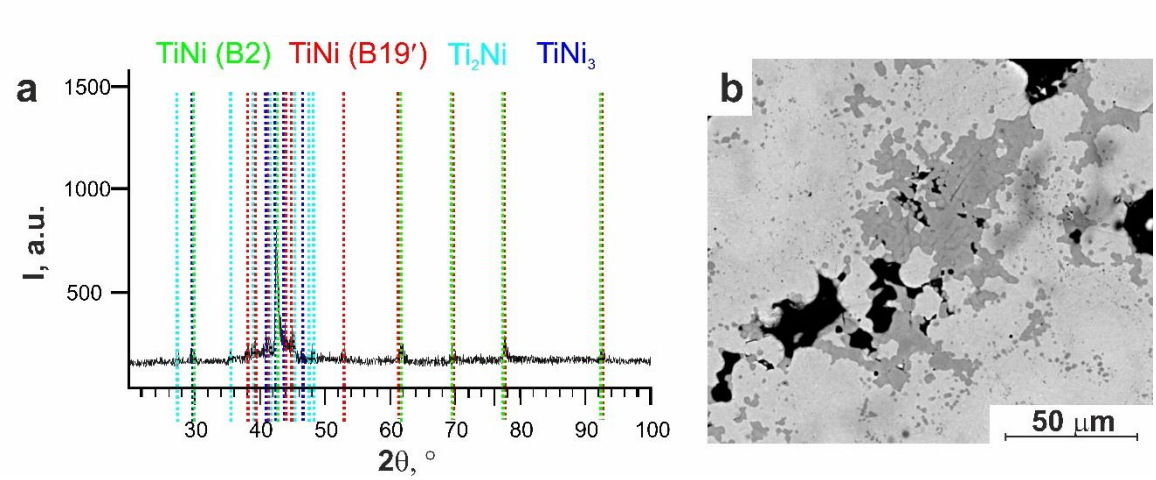

Figure 4. (**a**) XRD pattern of as-prepared porous SHS-produced TiNi alloy; (**b**) SEM image (BSE) of a thin section of porous SHS-prepared TiNi alloy showing phase distribution in the TiNi matrix.

The Ti_2Ni-type phases are not coherent with the TiNi matrix phase, which is why they have a significant effect on its physical and mechanical properties [27]. On the other hand, the TiNi matrix was previously shown to always contain such secondary phases irrespective of initial synthesis temperature of the alloy [27, 61]. In general, the use of elevated synthesis temperatures reduces the content of Ti_2Ni-type phases. Their particles are localized along grain boundaries in the form of thin layers and isolated precipitates (Figure 4b). Such layers are known as the predominant sites for crack propagation during fracture due to their incoherent connection with the matrix and relatively large dimensions. So, the presence of such Ti-rich secondary-phase particles is not desired in TiNi implants, since their presence has a negative effect on material's mechanical properties.

In light of the above, in the present work, to get rid of such Ti_2Ni-type surface inclusions, the SHS-produced TiNi material was etched in an aqueous solution of nitric and hydrofluoric acids. Along with the removal of undesired secondary-phase particles, etching was found to form a new topography of the material's pore walls, increasing their specific surface area and, subsequently, enhancing cell adhesion and growth on the implant surface.

3.1.3. Surface Modifications via Etching

Our choice of etchant was based on the analysis of literature devoted to methods for obtaining metallographic samples based on titanium and nickel alloys [33 – 37]. The etchant's composition was selected so that the Ti_2Ni and $Ti_4Ni_2(O,N,C)$ phases were subject to etching. During the interaction of both TiNi and Ti_2Ni-type phases with a mixture of nitric and hydrofluoric acids, similar products are formed according to reactions (1) and (2). A yellow-brown gas (NO_2) is released, and a solution of hexafluorotitanic acid ($H_2[TiF_6]$) and green ($Ni(NO_3)_2$ is formed. The latter hydrolyzes over time (reaction (3)) forming white insoluble precipitates of $TiO_2{\times}H_2O$.

$$TiNi + 6HF + 8HNO_3 = 6NO_2\uparrow + 6\,H_2O + Ni(NO_3)_2 + H_2[TiF_6] \quad (1)$$

$$Ti_2Ni + 12HF + 14HNO_3 = 12NO_2\uparrow + 12H_2O + Ni(NO_3)_2 + 2H_2[TiF_6] \quad (2)$$

$$H_2[TiF_6] + H_2O = TiO_2{\times}H_2O\downarrow + HF \quad (3)$$

Preprints (www.preprints.org) | NOT PEER-REVIEWED | Posted: 8 January 2024 doi:10.20944/preprints202401.0580.v1

Thus, both the TiNi matrix of the material and its secondary-phase inclusions (Ti_2Ni-type) overcome etching under certain conditions. To optimize the etching process and understand how it influences the final produce, the SHS-produced materials were etched in acidic media for up to 10 s and longer. Based on the results, several etching stages can be distinguished.

At the first stage of etching, lasting from 1 to 3 s in acidic environment, the oxycarbide layer was partially removed. Figure 5a shows a dendritic relief found underneath the removed layer. Micro-X-ray spectral analysis revealed that these areas were enriched in Ti (Figure S1, *Supplementary Materials*). A stream-like relief in the SEM image in Figure 5a is characteristic of incomplete removal of the oxycarbonitride layer, as was previously reported by Otsuka and coworkers [27].

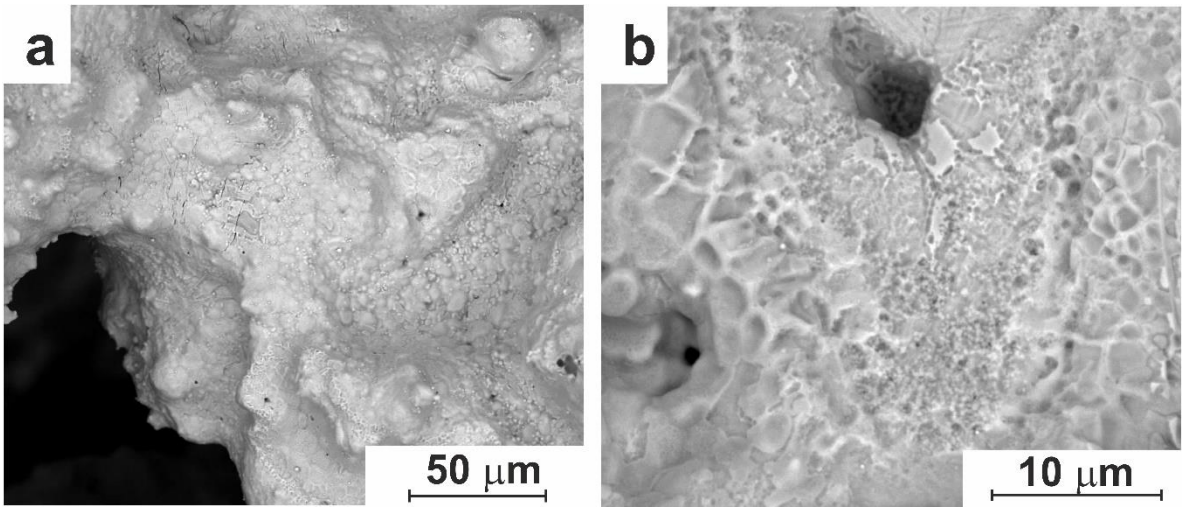

Figure 5. SEM images (BSE mode) of pore wall surface after first (**a**) and second (**b**) stages of etching.

At the second etching stage (3–7 s), inter-dendritic layers and second-phase particles were observed to be etched. As a result, microporous surfaces on the pore walls began to form, as seen in Figure 5b. At the same time, because of the presence of dendritic zones, the cellular relief of the pore wall surface is seen in Figure 5b to remain mainly unchanged. The thickness of the dendritic liquation zone for a finely porous SHS material ranges from 10 to 15 μm in different places. In areas where the thickness of such a dendritic layer is minimal, a microporous surface is formed after the dissolution of the dendrite body (TiNi matrix phase). In the other areas, etching proceeded by dissolving not only the dendritic bodies, but also the inter-dendritic layers (Figure 5b).

At the third stage of etching (7–10 s), the layer with the dendritic liquation zone was found to be removed from the pore wall surfaces. Also, single particles of secondary phases were also observed to be etched in the body of the grains of the TiNi matrix. This resulted in a pronounced rough microporous surface of the pore walls seen in Figure 6a, where changes in total material porosity were found to be as high as 68%. More specifically, when comparing the histograms of pore size distribution before and after etching for 10 s (Figure 6b), one can conclude that the fraction of small pores (below 100 μm) increased. Also, due to etching of larger pores, an increase in the maximum pore size to 1300 μm can be observed. At the same time, expectedly, the composition of the TiNi metal matrix, as revealed by XRD, remained essentially same as before etching, since only the pore wall surface was modified (Figure 6c).

Preprints (www.preprints.org) | NOT PEER-REVIEWED | Posted: 8 January 2024 doi:10.20944/preprints202401.0580.v1

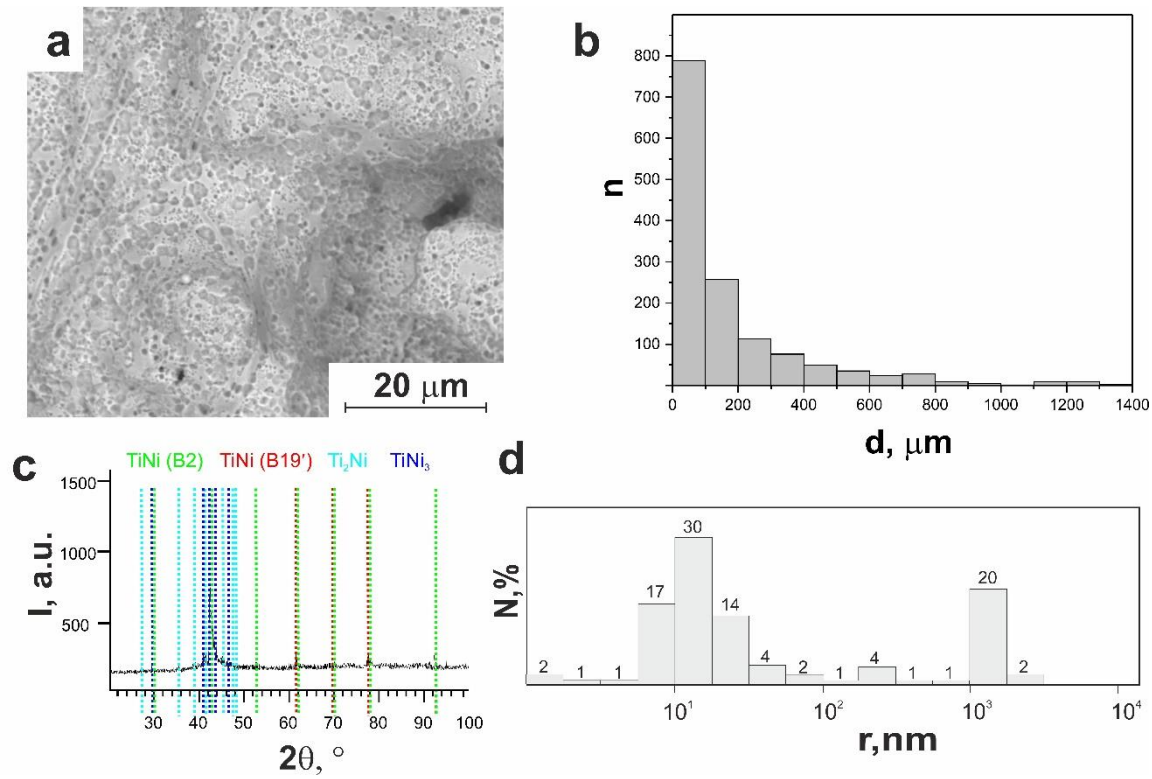

Figure 6. (**a**) SEM image (BSE mode) of the surface of pore walls, (**b**) histogram of pore size distribution, XRD pattern (**c**), and histogram of the micropore size distribution (**d**) in the porous TiNi alloy after the third stage of etching (7–10 s).

The mercury porosimetry revealed that after etching for 10 s, the number of micropores with sizes below 100 nm increased (Figure 6d). It is believed that such a structure of the pore wall surfaces should be more favorable for cell adhesion and growth, since the developed rough surface of the pore walls should facilitate and stimulate their attachment and further development on such a material based on TiNi [60–62].

Further etching (longer than 10 s) led to disruption of the regular porous structure of the material (Figure 7). At this stage, layer-by-layer etching of both the TiNi matrix and Ti-enriched particles resulted in formation of new pore wall surfaces with micropores. The macropores were found to significantly increase in size, and the metal matrix degraded because of active processes of dissolution of interpore bridges. Finally, dead-end pores were also found on the pore wall surfaces, with their own micropores inside (Figure 7). Therefore, based on the above discussion, 10 s was chosen as the optimum etching time for both cleaning and modifying the SHS-generated porous TiNi.

Thus, characterized thoroughly the structure and composition of both the initial (as-synthesized by means of SHS) and acid-modified porous TiNi, after which the optimal etching time was chosen to be 7–10 s. It allowed us to remove undesired particles of Ti_2Ni and $Ti_4Ni_2(O,C)$ phases from the pore walls and to structurally modify the surface of the final material, making it more attractive for cell and tissue adhesion during implantation. As shown below, the developed surface treatment of the SHS-produced TiNi material indeed modifies properly the pore space on its surface, which then significantly accelerates the bio-integration of the material after implanting.

Preprints (www.preprints.org) | NOT PEER-REVIEWED | Posted: 8 January 2024 doi:10.20944/preprints202401.0580.v1

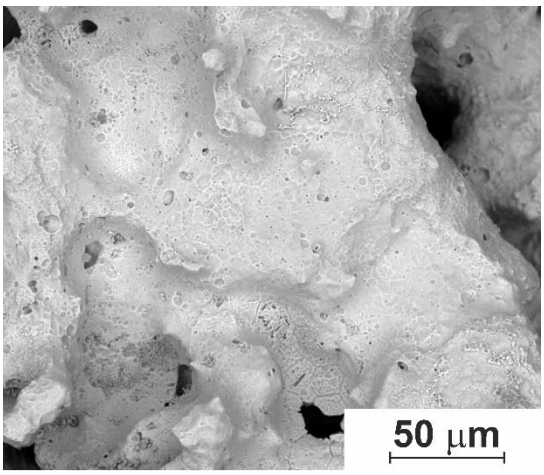

Figure 7. SEM image (BSE mode) of the pore wall surface of porous TiNi alloy after etching for longer than 10 s.

3.2. In Vitro Experiment

3.2.1. Cell Culture Cultivation

To study the biocompatibility of the modified TiNi material, bone marrow cells, which are adherent cells, were used. Since bone marrow cells are multipotent, the results obtained for such cells are believed to be also applicable to chondrogenic, osteogenic, adipogenic, neural and other cells derived from bone marrow mesenchymal stem cells. In the present work, the cultivation of bone marrow cells was carried out on samples of modified porous-permeable TiNi for as long as 21 days, and the results were collected after days 1, 7, 14, and 21.

On the first day of cultivation, active cell attachment was observed. The cells are seen in Figure 8a to have clear shapes and a smooth surface shell, which indicates the material's pore space provided favorable conditions for their adhesion. In some parts of the sample, both single cells and groups consisting of 3–5 cells can be observed. During subsequent growth of the cells, such agglomerates are known to develop more actively than single cells [63]. So, their appearance at early stages of implanting is quite desired.

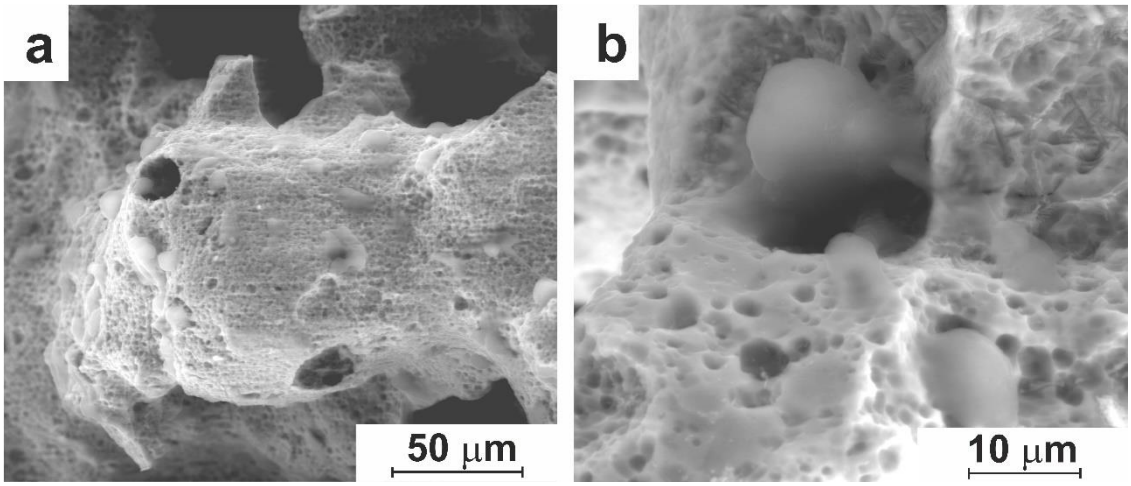

Figure 8. SEM images (low-vacuum SE mode) of surface space surface of the modified TiNi after day 1 of cell cultivation. (**a**) Cells adhered on the surface; (**b**) cells attached to pore walls with opposite-directed pseudopodia.

Figure 8 shows that on day one of experiment, some cells spread out and began to form short pseudopodia. The cells with pseudopodia attached at several locations on the walls of the micropore surface can be observed. Most of them, like the one in Figure 8b, have pseudopodia on their

Preprints (www.preprints.org) | NOT PEER-REVIEWED | Posted: 8 January 2024 doi:10.20944/preprints202401.0580.v1

diametrically opposite edges. Moreover, after attachment, such pseudopodia stretch the cell in different directions and flatten its shape, thus creating a large contact area with the microporous surface. The direction of movement of pseudopodia is determined by cell's internal signals. Accordingly, at early stages of development of the intercellular matrix, the cells are believed to move towards unoccupied areas, avoiding layering on each other [63, 64].

On day 7, accumulation of intercellular mass was detected, which constituted the prerequisites for even more active proliferation of cell colonies. A large number of cells were found inside the inner microporous surface of pore walls, often with clusters of cells that clearly imply their multiplication. The cell growth and multiplication were observed to be accompanied by the formation of thin surficial (Figure 9a) and thickened volumetric pseudopodia up to 50 μm in length (Figure 9b). At this stage, many cells were seen to be connected to each other by pseudopodia spreading over the surface (see Figure S2, *Supplementary Materials*). Many pseudopodia are seen in Figures 9a and b to create surface networks by now, as their number and that of cell fibers increased, implying the active development of the culture medium. Cell clusters of various sizes, as well as strands formed by clusters of cell fibers, pseudopodia and cells, were also observed.

As cultivation time elapsed from 7 to 14 days, the volume of grown cell mass inside the pore space of the material further increased. Cells were found to multiply, producing intercellular fibers and forming spatial cell processes with different shapes and sizes. The surface of the material was already well covered with an intercellular matrix by now, with the contours of pseudopodia still visible, such as those seen in Figure 9c. As the cellular ensemble developed, the formed structures thickened (Figure 9d).

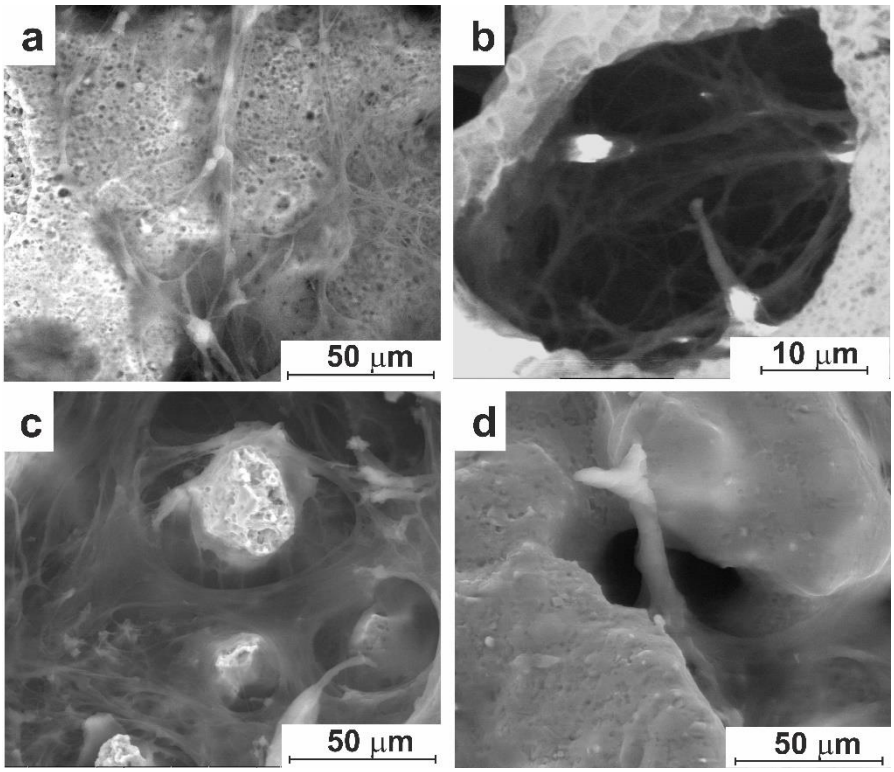

Figure 9. SEM images (low-vacuum SE mode) of the pore space of modified TiNi on day 7 of cell cultivation (**a, b**) and on day 10 (**c, d**). (**a**) Superficial development and (**b**) volumetric development; (**c**) thin surface layer with pseudopodia; (**d**) thickening of fibers.

After 14 days of cultivation, the microporous surface of pore walls is well-seen in Figure 10a,b to be filled with cells and intercellular fibers. Cell colonies are now seen to line up along the inner surface of the pores and fill in the free pore space; and the grown cell culture is now changing from surface to bulk type. Numerous cell clusters that represent multiplication centers, as well as intercellular fibers and more massive pseudopodia, are also seen in Figure 10a,b.

Preprints (www.preprints.org) | NOT PEER-REVIEWED | Posted: 8 January 2024 doi:10.20944/preprints202401.0580.v1

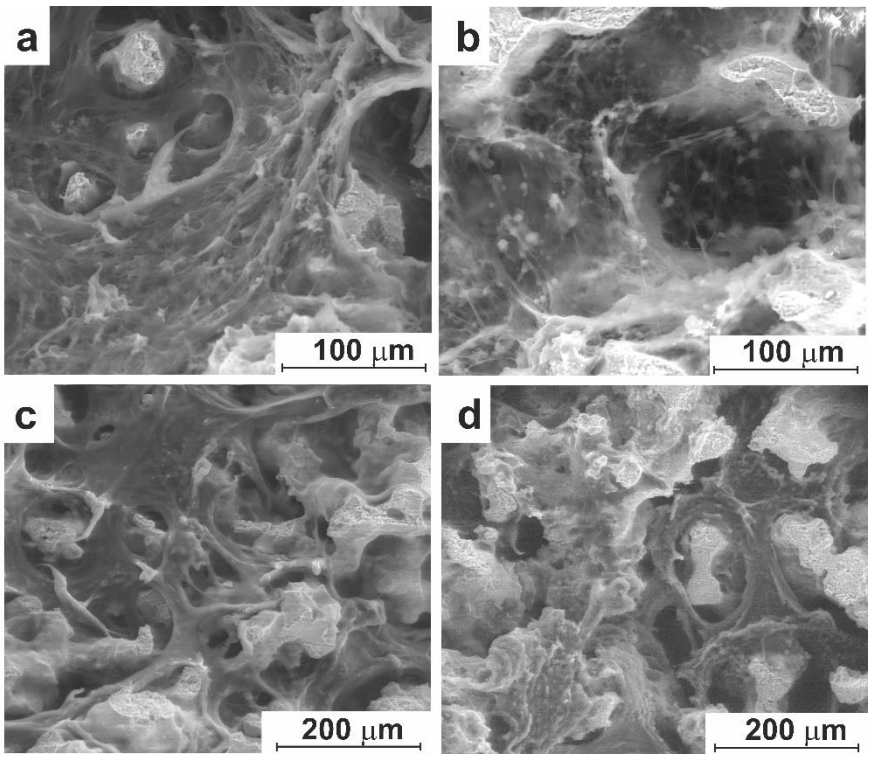

Figure 10. SEM images (low-vacuum SE mode) of the morphology of cell culture observed on the surface of modified porous TiNi material after 14 (**a, b**) and 21 (**c, d**) days of cultivation. (**a**) Cells in small surface pores; (**b**) cells in large pores; (**c**) formed tissue adjacent to pore wall surface; (**d**) pore space is fully filled by high-density mature tissue.

At this stage, there was a clear difference observed between cell populations grown in surface pores with different sizes. More specifically, cells were found to populate smaller pores more readily as the volume of such pores was favorable for their pseudopodium development and spatial fiber formation. As a result, pores smaller than 200 μm in size were completely filled in, as well seen in Figure10a, after which the formation of tissue structures began. At the same time, the cell growth in larger pores is seen in Figure 10b to be much slower, probably because such larger pores do not facilitate the transition from surface to volume filling of the pore. Hence, the resulting tissue observed in larger pores consisted of two structural elements, cells and intercellular fibers, which became massive and acquired high density over cultivation time.

By day 21, the number of cells and fibers of the formed intercellular matrix further increased, as seen in Figure 10c,d. The porous TiNi material was found to be filled by compact cellular structures, and further signs of the formation of connective tissue in the pore space are well seen by now. More specifically, about 80% of the internal space is seen in Figure 10c to be filled with formed tissue which is generally adjacent to the pore wall surface. The tissue was formed layer-by-layer on the pore wall surface, and its characteristic texture is seen in Figure 10d. At this point in time, the porous TiNi material is not visible through the formed dense tissue, yet some cells are seen in Figure 10d to retain their contours, being an integral part of mature tissue together with fibers. Accordingly, after 21 days, complete formation of resulting tissue structure was observed, with pore space of the tested TiNi material fully filled by high-density tissue.

Thus, our detailed study of the interaction of modified porous permeable TiNi with bone marrow cells demonstrated that the surface of this material is well adhesive and biocompatible with this type of cells. The process of integration of cell culture can be divided into several stages which differ in duration and depend on the cultivation conditions: (i) cell adhesion (attachment); (ii) development of pseudopodia; (iii) cell growth and reproduction; (iv) development of intercellular mass; (v) compaction of cellular structures (cells, pseudopodia, fibers); and (vi) tissue formation. All these stages were observed on material's surface during 21 days of testing. At the same time, the

Preprints (www.preprints.org) | NOT PEER-REVIEWED | Posted: 8 January 2024 doi:10.20944/preprints202401.0580.v1

stages proceeded differently at different surface locations, i.e., inside small and larger wall pores of the sample. More specifically, the small pores were found to exhibit faster and more intense tissue formation on their surface.

Therefore, one can conclude that high integration connection of bone marrow cells with the modified porous-permeable material based on TiNi was observed. This implies that this material can potentially be successfully used for manufacturing implants, including orbital ones, for their use in ophthalmology.

3.3. In-Vivo Studies

3.3.1. Experiment on Animals

The biocompatibility of novel modified porous-permeable TiNi was studied in *in- vivo* experiments on animals (20 dogs). After evisceration of the eyeball, its musculoskeletal stump with an orbital implant made of modified TiNi was formed.

Figure 11a shows that after implanting for 10 days, a capsule of loose soft-fibrous connective tissue formed around an orbital implant. The pore space of the TiNi material is seen to be filled with clusters of actively developing cells, as well as with cellular collagen fibers growing from the periphery to the center and gradually filling the entire volume of the implant (Figure 11b). Figure 11c reveals that the fibers of immature connective tissue completely cover the inside surface of the pores and form an intertwined chaotic network inside the pore space. Such fibers are known to be waste products of actively dividing and migrating fibroblasts.

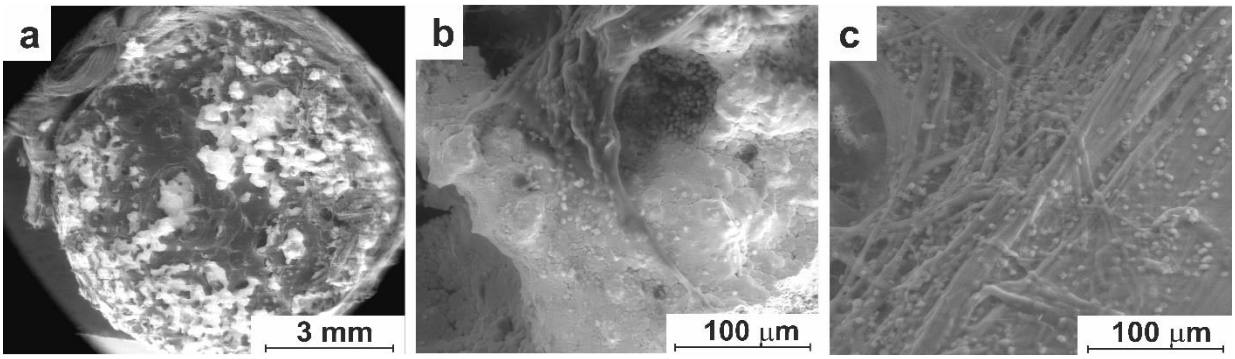

Figure 11. SEM images (low-vacuum SE mode) of orbital implant made of acid-modified porous TiNi material after 10 days of implantation: (**a**) capsule around the implant and filling of pore space with connective tissues; (**b**) individual fibroblasts and cell clusters; (**c**) network of fibers of immature connective tissue.

In addition to the accumulation of cells and fibrous structures, newly formed vessels were also observed in the pores of the implant (Figure 11b). Altogether, the cells, their clusters, fibrous areas, and newly formed vessels can be considered a sufficient sign, or identifying elements, of a loose connective tissue.

After 30 days from the beginning of the experiment, the capsule around the implant was found to become denser. It had a structure of mature connective tissue as thick as up to 500 μm. The thickness of the capsule did not increase during the maturation of connective tissue that constituted it. Some of the collagen fibers found on the pore wall surface and inside the pore space are seen in Figure 12 to be compacted and well arranged, while some others are located chaotically. Surrounded by fibers, individual cells of a fibroblast series can also be visualized in Figure 12a. The vessels seen in Figure 12b were formed on the pore surface and in the volume of the implant.

Preprints (www.preprints.org) | NOT PEER-REVIEWED | Posted: 8 January 2024 doi:10.20944/preprints202401.0580.v1

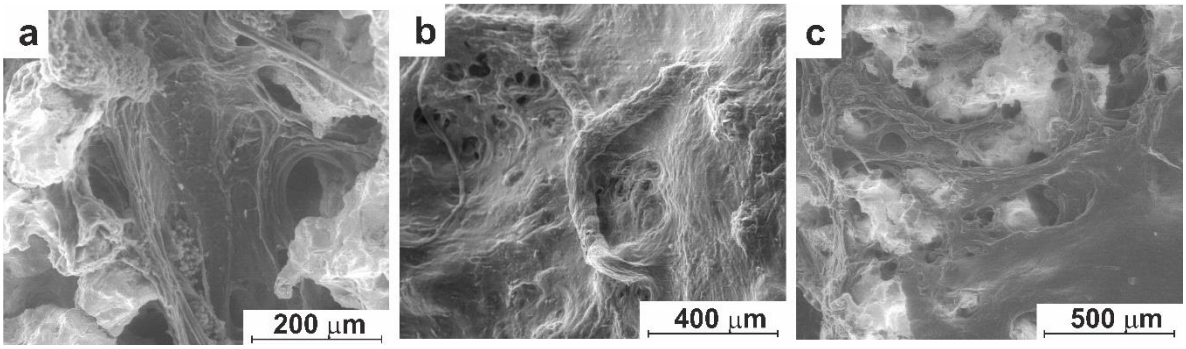

Figure 12. SEM images (low-vacuum SE mode) of orbital implant made of modified porous TiNi material after 30 days of implantation: (**a**) collagen fibers with individual cells; (**b**) vessels on implant surface; (**c**) connective tissue in implant's pores.

The cell mass was found to get gradually more compact, dense and thicker. The cell mass, with all its structural elements that are now well observed inside the implant pore space, indicates the transformation of a loose connective tissue into a mature and dense one. At this stage, almost all the pores of the implant are filled with such a mature connective tissue (Figure 12c), which results in diffuse tissue colonization of the implant.

As seen in Figure 13a, on day 90 after surgery, the connective tissue capsule on the surface of the implant was found to become denser and thinner than before, which indicates the absence of cytotoxicity of the implanted material. The connective tissue inside the implant pores continued to develop, showing predominance of fibrous component by this point in time (see Figure 13a). At the same time, cellular fibers became denser, being located randomly on the surface and in the pore volume, while relatively bulky fibrous areas formed mainly by intertwined cell fibers, as well seen in Figure 13a. The development of vascular system, as well as single fibroblasts, can be found at this stage. The formed connective tissue is characterized by good adhesion to the surface of the implant pore wall; it fits tightly to the pore wall, closely following its relief.

In general, the tissue observed on the pore wall surface and inside the implant pore space after 30 and 90 days was structurally similar. It consisted of the same structural elements, namely, cells, their clusters, cell fibers, fibrous areas, and vessels. Over time, however, it gradually developed, forming a mature-type connective tissue. Eventually, the observed invariance in time of the resultant tissue indicates that the bio-integration of the orbital implant tested in our work is characterized by high rates of cell colonization and takes no more than 30 days.

After 180 days of implanting, the capsule seen on the implant surface was poorly identified. As seen in Figure 13b,c, the fibrous areas in the pore space of the implant merged into a homogeneous mass, and a dense connective tissue formed.

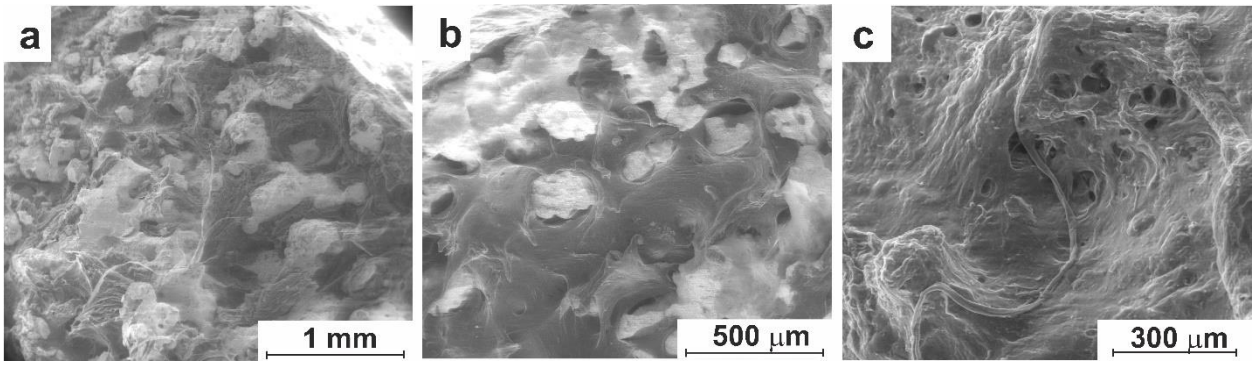

Figure 13. SEM images (low-vacuum SE mode) of orbital implant made of modified porous TiNi material after 90 (**a**) and 180 (**b, c**) days of implantation: (**a**) tissue location in the pore space; (**b**) fully formed connective tissue; (**c**) vessels in a dense connective tissue.

 doi:10.20944/preprints202401.0580.v1

Thus, by the end of the first month after implanting, the structural elements of cellular mass developed in the pore space of the implant, with a connective tissue gradually transforming from loose to dense. On days 30, 90, and 180 from the beginning of the experiment, the formed tissue was found to be structurally identical, with almost all implant pores well-filled with a mature connective tissue. This implies active bio-integration of the orbital implant with body tissues, accompanied with the formation of reliable connections between the implant and the surrounding anatomical structures, all being largely established within one month after surgery.

4. Conclusions

This work reports on a porous SHS-prepared TiNi material for ophthalmological implants. Both the as-prepared and acid-modified porous materials with different states of the pore space and porosity coefficients were first thoroughly characterized. The modification method employed to modify the material's surface morphology was based on chemical etching with removal of the Ti_2Ni and $Ti_4Ni_2(O,C)$ secondary-phase particles located on the pore wall surfaces.

It was demonstrated that after chemical etching there was an increase in the number of micropores less than 100 nm in size. After etching, the obtained rough surface of pore walls was more suitable for the attachment and development of cell cultures. *In-vitro* studies of the dynamics of integration of cellular material showed that cell growth and integration were improved on the acid-treated material with rougher surface of its pore walls.

Bio-integration of an orbital implant made of the acid-modified porous-permeable TiNi was also studied *in vivo*, and the reaction to its presence by body tissues was monitored over time. The process of integration of such a porous permeable implant was found to be accompanied by a high degree of adhesion of cellular and tissue structures of newly formed tissues into the material's pore space. Formation of a reliable connection between the implant and surrounding anatomical structures was ensured within one month after surgery.

Thus, the high ability for bio-integration in a combination with its good framework properties make the novel acid-modified porous-permeable TiNi an attractive material for creating orbital implants for the formation of musculoskeletal stumps of the eyeball after evisceration. The material demonstrated a high degree of integration and tissue-implant connections, which is expected to provide its strong fixation in tissues, stable volume and shape of the musculoskeletal stump of the eyeball, and reduced risk of exposure and rejection of the implant.

Supplementary Materials: The following supporting information can be downloaded at: www.mdpi.com/xxx/s1, Figure S1: EDX spectrum taken on the surface of TiNi after first stage of etching (1-3 s) showing its enrichment in Ti; Figure S2: SEM images (low vacuum SE mode) of the pore space of modified TiNi on day 7 of cell cultivation. Many cells are seen to be connected to each other by pseudopodia spreading over the surface at different magnifications: (a) 500x; (b) 2000x; (c) 8000x.

Author Contributions: Conceptualization, S.G.A. and V.N.H.; methodology, M.I.K.; validation, S.A.K. and A.V.S.; soft-ware, S.A.K., N.V.A and A.V.S.; visualization, E.N.T. and A.V.S.; formal analysis, S.A.K. and E.A.B.; investigation, S.G.A., V.N.H., N.V.A, E.N.T. and M.I.K.; resources, V.N.H.; data curation, S.P., V.P. and Y.A.M.; writing—original draft preparation, S.G.A.; writing—review and editing, S.G.A., A.V.S., S.A.K. and V.N.H.; supervision, V.E.G; project administration, S.G.A.; funding acquisition, S.G.A. All authors have read and agreed to the published version of the manuscript.

Funding: The study was supported by the Russian Science Foundation (grant no. 19-79-10045). https://rscf.ru/project/19-79-10045/.

Institutional Review Board Statement: All procedures involving animals were carefully carried out with strict adherence to the Helsinki Declaration of 1975 and in accordance with the European Community's Council Directive 86/609/EEC. The study protocols were officially approved (approval code number 20/1116/2017 of 5 May, 2017) by the Bioethical Committee of Tomsk State University and by the Bioethical Committee of Kuzbass Regional Clinical Hospital (approval code number 138/1 of 16 March 2023).

Data Availability Statement: Not applicable.

Acknowledgments: S.A.K. thanks the support from the Amada Foundation (grant no. AF-2019225-B3).

Conflicts of Interest: The authors declare no conflict of interest.

References

1. Chen, X.Y.; Yang, X.; Fan, X.L. The Evolution of Orbital Implants and Current Breakthroughs in Material Design, Selection, Characterization, and Clinical Use. *Front. Bioeng. Biotechnol.* **2022**, *9*, 1–14. doi:10.3389/fbioe.2021.800998
2. Migliori, M.E. Enucleation versus Evisceration. *Curr. Opin. Ophthalmol.* **2002**, *13*, 298–302. doi: 10.1097/00055735-200210000-00002
3. Hui, J. Outcomes of orbital implants after evisceration and enucleation in patients with endophthalmitis. *Curr. Opin. Ophthalmol.* **2010**, *21*, 375-379. doi: 10.1097/ICU.0b013e32833b7a56
4. Gundorova, R.A. *Traumas of the Eye.*; GEOTAR-Media: Moscow, Russia, 2014; p. 560. (In Russian)
5. Filatova, I.A.; Mokhammad, I.M. The modified method for evisceration in the case of buphthalmos with the use of a combination of orbital implants. *Russian Pediatric Ophthalmology* **2017**, *12*, 210-215, doi:10.18821/1993-1859-2017-12-4-210-215. (In Russian)
6. Castela, G. *Manual of Ophthalmic Plastic and Reconstructive Surgery*, 1st ed.; Sociedade Portuguesa de Oftalmologia: Lisbon, Portugal, 2016; p. 308
7. Ruchi, D. S.; Ramesh, M. S.; Vinay, A.; Setabutr, P. Evisceration and Enucleation: A National Survey of Practice Patterns in the United States. *Ophthalmic Surg. Lasers Imaging* **2012**, *43*, 425–430. doi:10.3928/15428877-20120725-01
8. Verigo, E.N.; Gundorova, R.A.; Sadovskaya, E.P. A comparative study of the stump and prosthesis mobility depending on the technique of eye enucleation. *Russian Ophthalmological Journal* **2012**, *5*, 14-19. (In Russian)
9. Luzjanina, V.V.; Egorov, V.V.; Smoljakova, G.P. Study of the properties of implants for oculomotor ocular stump grafting. *Vestnik of the Orenburg State University* **2009**, *12*, 84-87. (In Russian)
10. Naumenko, L.V.; Malinovskii, G.F.; Krasnyi, S.A.; Zhilyaeva, E.P. The use of allotransplant from the subcutaneous fat with plantar aponeurosis for the musculoskeletal stump formation during enucleation. *Novosti Khirurgii* **2021**, *29*, 191-197. DOI:10.18484/2305-0047.2021.2.191 (In Russian)
11. Schirmer, K.E.; Raphael, S.S. Ocular Reactions to Plastic Materials (Polyethylene and Teflon). *Am. J. Ophthalmol.* **1961**, *52*, 61–65. doi:10.1016/0002-9394(61)90453-6
12. Schmitzer, S.; Simionescu, C.; Alexandrescu, C.; Burcea, M. The Anophthalmic Socket - Reconstruction Options. *J. Med. Life* **2014**, *7*, 23–29
13. Astakhov Yu.S., Nikolajenko V.P., D'yakov V. E. The use of PTFE implants in ophthalmology.; Foliant: Sankt-Peterburg, Russia, 2007; p. 256. (In Russian)
14. Tsurova, L.M.; Milyudin, E.S. Comparative analysis of using different orbital implants to form postenucleational locomotor stump. *Vestnik of the Orenburg State University* **2014**, *12*, 334-337. (In Russian)
15. Ivolgina, I.V. The peculiarities of the use of different implants in musculoskeletal stump formation after enucleation. *Tambov University Reports. Series Natural and Technical Sciences* **2015**, *20*, 577-580. (In Russian)
16. Chalasani, R.; Poole-Warren, L.; Max Conway, R.; Ben-Nissan, B. Porous Orbital Implants in Enucleation: A Systematic Review. *Surv. Ophthalmol.* **2007**, *52*, 145–155. doi:10.1016/j.survophthal.2006.12.007
17. Custer, P.L.; Kennedy, R.H.; Woog, J.J.; Kaltreider, S.A.; Meyer, D.R. Orbital Implants in Enucleation Surgery A Report by the American Academy of Ophthalmology. *Ophthalmol.* **2003**, *110*, 2054–2061. doi:10.1016/S0161-6420(03)00857-1
18. Shoamanesh, A.; Pang, N.K.; Oestreicher, J.H. Complications of Orbital Implants: A Review of 542 Patients Who Have Undergone Orbital Implantation and 275 Subsequent PEG Placements. *Orbit* **2007**, *26*, 173–182. doi:10.1080/01676830701555204
19. Yoon, J. S.; Lew, H.; Kim, S. J.; S.Y.Lee. Exposure Rate of Hydroxyapatite Orbital Implants: A 15-Year Experience of 802 Cases. *Ophthalmology* **2008**, *115*, 566-572.e2. doi:10.1016/j.ophtha.2007.06.014
20. Filatova, I.A.; Verigo, E.N.; Pryahina, I.A. Ophthalmectomy: characteristics of ophthalmic pathology, clinical manifestation of mechanical trauma, time constraints and methods of surgery. *Head and Neck Russian Journal* **2014**, *3*, 30-35. (In Russian)
21. Grusha, la. O.; Fedorov, A.A.; Baranov, P. Yu.; Bakayeva, T.V.; Pavlyuk, A.S. Study of the three-dimensional structure and biointegrative characteristics of porous orbital implant materials. *Vestnik Oftalmologii* **2010**, *126*, 9-13. (In Russian)
22. Alwitry, A.; West, S. K.; King, J.; Foss, A.J.; Abercrombie L.C. Long-Term Follow-up of Porous Polyethylene Spherical Implants After Enucleation and Evisceration. *Ophthal. Plast. Reconstr. Surg.* **2007**, *23*, 11–15. doi:10.1097/01.iop.0000249429.02757.6b
23. Dziubla, T.D.; Lowman, A.M. Vascularization of PEG-Grafted Macroporous Hydrogel Sponges: A Three-Dimensional in Vitro Angiogenesis Model Using Human Microvascular Endothelial Cells. *J. Biomed. Mater. Res.* **2004**, *68*, 603–614. doi:10.1002/jbm.a.20023

24. Gorbunova, Y.A.; Krivosheina, O.I.; Zapuskalov, I.V. Implant of porous titanium nickelide impregnated with autologous blood monocytes for the formation of orbital stump in the experiment. *Bulletin of Siberian Medicine* **2011**, *10*, 12-14. https://doi.org/10.20538/1682-0363-2011-4-12-14 (In Russian)
25. Gunther, V.E.; Khodorenko, V.N.; Chekalkin, T.L. Medical Materials with Shape Memory. *In Medical Materials and Shape Memory Implants*, 1st ed.; NPP «MIC»: Tomsk, Russia, 2011; p. 534. (In Russian)
26. Zapuskalov, I.V.; Gyunter, V.E.; Steblyuk. *Shape memory implants in ophthalmology*, NPP «MIC»: Tomsk, Russia, 2012; p. 189. (In Russian)
27. Otsuka, K.; Ren, X. Physical metallurgy of TiNi based shape memory alloys. *Prog. Mater Sci.* **2005**, *50*, 511–678
28. Tosun, G.; Ozler, L.; Kaya, M.; Orhan, N. A Study on Microstructure and Porosity of NiTi Alloy Implants Produced by SHS. *J. Alloys Compd.* **2009**, *487*, 605–611. doi:10.1016/j.jallcom.2009.08.023
29. Zhang, J.; Fan, G.; Zhou, Y.; Xiangdong D.; Otsuka, K.; Nakamura, K.; Sun, J.; Ren, X. Does Order-Disorder Transition Exist in near-Stoichiometric Ti-Ni Shape Memory Alloys. *Acta Mater.* **2007**, *55*, 2897–2905. doi:10.1016/j.actamat.2006.12.028
30. Saldan, I.; Frenzel, J.; Shekhah, O.; Chelmowski, R.; Birkner, A.; Wöll, Ch. Surface of Ti-Ni Alloys after Their Preparation. *J. Alloys Compd.* **2009**, *470*, 568–573. doi:10.1016/j.jallcom.2008.03.050
31. Lelatko, J.; Freitag, M.; Rak, J.; Wierzchoń, T.; Goryczka, T. Structure. of Nitride and Nitride/Oxide Layers Formed on NiTi Alloy. *Solid State Phenom.* **2012**, *186*, 259–262. doi:10.4028/www.scientific.net/SSP.186.259.
32. Chu, C.L.; Wang, R.M.; Hu, T.; Yin, L.H.; Pu, Y.P.; Lin, P.H.; Wu, S.L.; Chung, C.Y.; Yeung, K.W.K.; Chu, P. K. Surface Structure and Biomedical Properties of Chemically Polished and Electropolished NiTi Shape Memory Alloys. *Mater. Sci. Eng.* **2008**, *28*, 1430–1434. doi:10.1016/j.msec.2008.03.009
33. Che, H.; Ma, Y.; Fan, Q.-C. Investigation of the Mechanism of Self-Propagating High-Temperature Synthesis of TiNi. *J. Mater. Sci.* **2011**, *46*, 2437–2444. doi:10.1007/s10853-010-5090-3
34. Tang, C.Y.; Zhang, L.N.; Wong, C.T.; Chan, K.C.; Yue, T.M. Fabrication and Characteristics of Porous NiTi Shape Memory Alloy Synthesized by Microwave Sintering. *Mater. Sci. Eng. A.* **2011**, *528*, 6006–6011. doi:10.1016/j.msea.2011.04.040
35. Jani, J.M.; Leary, M.; Subic, A.; Gibson, M.A. A Review of Shape Memory Alloy Research, Applications and Opportunities. *Mater. Des.* **2014**, *56*, 1078-1113. doi:10.1016/j.matdes.2013.11.084
36. Black, J.; Hastings, G. *Handbook of Biomaterial Properties*; Springer: Boston, MA, USA, 1998; p. 590
37. Bansiddhi, A.; Sargeant, T.D.; Stupp, S.I.; Dunand, D.C. Porous NiTi for Bone Implants: A Review. *Acta Biomater.* **2008**, *4*, 773–782. doi:10.1016/j.actbio.2008.02.009
38. Ayers, R. A.; Burkes, D.; Gottoli, G.; Yi, H.C.; Moore, J.J. The Application of Self-Propagating High-Temperature Synthesis of Engineered Porous Composite Biomedical Materials. *Mater. Manuf. Process.* **2007**, *22*, 481–488. doi:10.1080/10426910701235967
39. Kang, S.-B.; Yoon, K.-S.; Kim, J.-S.; Nam, T.-H. Smart Materials-Fundamentals and Applications. In Vivo Result of Porous TiNi Shape Memory Alloy: Bone Response and Growth. *Mater. Trans.* **2002**, *43*, 1045-1048. DOI:10.2320/matertrans.43.1045
40. Li, J.; Panton, B.; Mao, Y.; Dawood, N.M.; Kadhum, A.-R.; Ali, A.; Atiyah, A.A. Fabrication of Porous NiTi Shape Memory Alloy Objects by Powder Metallurgy for Biomedical Applications. *Mater. Des.* **2009**, *30*, 4483–4487. doi:10.1088/1757-899X/518/3/032056
41. Lagoudas, D.C.; Vandygriff, E.L. Processing and Characterization of NiTi Porous SMA by Elevated Pressure Sintering. *J. Intell. Mater. Syst. Struct.* **2002**, *13*, 837–850. doi:10.1177/1045389X02013012009
42. Anikeev, S.; Hodorenko, V.; Chekalkin, T.; Gunther, V. E.; Kang, J.-H.; Kim, J.-S. Fabrication and Study of Double Sintered TiNi-Based Porous Alloys. *Smart Materials and Structures* **2017**, *26*, 057001. doi:10.1088/1361-665X/aa681a
43. Yuan, B.; Zhu, M.; Chung, C.Y. Biomedical Porous Shape Memory Alloys for Hard-Tissue Replacement Materials. *Materials (Basel).* **2018**, *11*, 1716. doi:10.3390/ma11091716
44. Zheng, J.; Chen, L.; Chen, D.; Shao, C.; Yi, M.; Zhang, B. Effects of Pore Size and Porosity of Surface-Modified Porous Titanium Implants on Bone Tissue Ingrowth. *Trans. Nonferrous Met. Soc. China* **2019**, *29*, 2534–2545. doi:10.1016/S1003-6326(19)65161-7
45. Bansiddhi, A.; Sargeant, T.D.; Stupp, S.I.; Dunand, D.C. Porous NiTi for Bone Implants: A Review. *Acta Biomater.* **2008**, *4*, 773–782. doi:10.1016/j.actbio.2008.02.009
46. Ryan, G.; Pandit, A.; Apatsidis, D.P. Fabrication Methods of Porous Metals for Use in Orthopaedic Applications. *Biomaterials* **2006**, *27*, 2651–2670. doi:10.1016/j.biomaterials.2005.12.002
47. Shishkovsky, I. V; Volova, L.T.; Kuznetsov, M. V; Morozov, Y.G.; Parkin, I.P. Porous Biocompatible Implants and Tissue Scaffolds Synthesized by Selective Laser Sintering from Ti and NiTi. *J. Mater. Chem.* **2008**, *18*, 1309–1317. doi:10.1039/b715313a
48. Meisner, L.L.; Markov, A.B.; Proskurovsky, D.I.; Rotshtein, V.P.; Ozur, G.E.; Meisner, S.N.; Yakovlev, E.V.; Poletika, T.M.; Girsova, S.L.; Semin, V.O. Effect of inclusions on cratering behavior in TiNi shape memory alloys irradiated with a low-energy, high-current electron beam. *Surf. Coatings Technol.* **2016**, *302*, 495–506. https://doi.org/10.1016/j.surfcoat.2016.06.036

49. Meisner, L.L.; Markov, A.B.; Rotshtein, V.P.; Ozur, G.E.; Meisner, S.N.; Yakovlev, E.V.; Gudimova, E.Y. Formation of microcraters and hierarchically-organized surface structures in TiNi shape memory alloy irradiated with a low-energy, high-current electron beam. *AIP Conf. Proc.* **2015**, *1683*, 020145. https://doi.org/10.1063/1.4932835
50. Ashby, M.F. Materials Selection in Mechanical Design, 1st ed.; Butterworth-Heinemann: Oxford, UK, 2011; p. 513
51. Saldan, I.; Frenzel, J.; Shekhah, O.; Chelmowski, R.; Birkner, A. Surface of Ti-Ni Alloys after Their Preparation. *J. Alloys Compd.* **2009**, *470*, 568–573, doi:10.1016/j.jallcom.2008.03.050
52. Badr, M.; Mohammadzadeh, A.; Khalil-Allafi, J.; Khoshghadam-Pireyousefan, M.; Mostafaei, A. In-situ formation of TiN-TiO2 composite layer on NiTi shape memory alloy via fluidized bed reactor. *Ceramics International* **2020**, *46*, 21097-21106. https://doi.org/10.1016/j.ceramint.2020.05.184
53. Mehrvarz, A.; Khalil-Allafi, J.; Etminanfar, M.; Mahdavi, S. The study of morphological evolution, biocorrosion resistance, and bioactivity of pulse electrochemically deposited Hydroxyapatite/ZnO composite on NiTi superelastic alloy. *Surf. Coat. Technol.* **2021**, *423*, 127628. https://doi.org/10.1016/j.surfcoat.2021.127628
54. Zhao, X.; Sun, H.; Lan, L.; Huang, J.; Zhang, H.; Wang, Y. Pore structures of high-porosity NiTi alloys made from elemental powders with NaCl temporary space-holders. *Materials Letters* **2009**, *63*, 2402-2404. https://doi.org/10.1016/j.matlet.2009.07.069
55. Bansiddhi, A.; Dunand, D.C. Shape-memory NiTi foams produced by replication of NaCl space-holders. *Acta Biomaterialia* **2008**, *4*, 1996-2007. https://doi.org/10.1016/j.actbio.2008.06.005
56. Resnina, N.; Rubanik jr., V.; Rubanik, V.; Belyaev, S.; Bysha, V.; Kalganov, V.; Chepela. D. Influence of pre-heating temperature and ultrasonic vibration treatment on the structure and martensitic transformations in NiTi foams produced by SHS. *Lett. Mater.* **2022**, *12*, 164-168. https://doi.org/10.22226/2410-3535-2022-2-164-168
57. Resnina, N.; Palani, I.A.; Belyaev, S.; Singh, S.; Liulchak, P.; Karaseva, U.; Mani Prabu, S.S.; Jayachandran, S.; Kalganov, V.; Iaparova, E.; Demidova E. Influence of Heat Treatment on the Structure and Martensitic Transformation in NiTi Alloy Produced by Wire Arc Additive Manufacturing. *Materialia* **2021**, *20*, 101238, doi:10.1016/j.mtla.2021.101238
58. Bandyopadhyay, A.; Mitra, I.; Avila, J.D.; Upadhyayula, M.; Bose, S. Porous metal implants: processing, properties, and challenges. *Int. J. Extrem. Manuf.* **2023**, *5*, 032014. https://doi.org/10.1088/2631-7990/acdd35
59. Hiemenz, P.C. *Foundations of Colloid Science*, 3rd ed.; Marcel Dekker: New York, USA, 1997; p. 650
60. Che, H.-Q.; Ma, Y.; Fan, Q.-C. Investigation of the mechanism of self-propagating high-temperature synthesis of TiNi. *J Mater Sci.* **2011**, *46*, 2437–2444. https://doi.org/10.1007/s10853-010-5090-3
61. Gunther, V.E.; Khodorenko, V.N.; Chekalkin, T.L. Problems of biocompatibility of metallic materials. *Implants with Shape Memory* **2011**, *1–2*, p. 5–16. (In Russian)
62. Itin, V.I.; Pribytkov, G.A.; Khlusov, LA.; Zagrebin, L.V.; Shestov, S.S. Implant-carrier of cells made of porous permeable titanium. *Cellular Transplantation and Tissue Engineering* **2006**, *1*, 59-63. (In Russian)
63. Anderson, A.R.A.; Chaplain, M.A.J.; Rejniak, K. A.; Fozard J.A. Single-Cell-Based Models in Biology and Medicine. *Mathematical Medicine and Biology. A Journal of the IMA* **2008**, *25*, 185–186. https://doi.org/10.1093/imammb/dqn008
64. Vasiliev, Y. M. Cell as an architectural miracle. Cytoskeleton, capable of feeling and remembering. *Soros Educational Journal. Biology* **1996**, *4*, 4-10 (In Russian)